ACI STRUCTURAL JOURNAL TECHNICAL PAPER

Title No. 118-S85

Behavior of Alkali-Silica Reaction-Affected Reinforced Concrete Elements Subjected to Shear

by Anca C. Ferche and Frank J. Vecchio

Past research on the effects of alkali-silica reaction (ASR) on the behavior of shear-critical concrete structures have yielded contradictory results, whether they have come from full-scale tests on specimens extracted from existing ASR-affected structures or from laboratory specimens conditioned to accelerate the rate of the reaction. Both increases and decreases in the shear capacity of ASR-affected specimens were reported, when compared with either corresponding control specimens or theoretical strength.

Experiments were performed to better characterize the response of ASR-affected reinforced concrete. Ten panels were constructed and tested under in-plane pure shear loading conditions. The panels, containing varying amounts of in-plane and out-of-plane reinforcement, were cast with either non-reactive aggregate, reactive fine aggregate (Jobe-Newman), or reactive coarse aggregate (Spratt). To accelerate the rate of the reaction, the specimens were conditioned under elevated humidity and temperature. Test results indicated that the load capacity of the panels was not adversely affected by ASR strains ranging between 1.2×10^{-3} and 2.5×10^{-3}, as measured on corresponding standard expansion prisms, and that the shear stress at first cracking was in fact elevated. The panels' deformation capacity, however, was reduced by approximately 30% for the reactive specimens compared to similar non-reactive ones.

Keywords: alkali-silica reaction; ductility reduction; reinforced concrete; shear capacity.

INTRODUCTION

With increasing frequency, aging infrastructure displays signs of distress associated with severe deterioration mechanisms that could not have been anticipated during the design phase. Alkali-silica reaction (ASR) is one of the most harmful distress mechanisms affecting the performance of concrete structures worldwide. Deleterious ASR develops when the concrete mixture contains aggregate susceptible to alkali attack. The chemical reactions between the alkali hydroxides from the cement paste and certain siliceous minerals produce a gel that swells in the presence of moisture, leading to pressure buildup that causes macroscopic expansion. Since it was first identified by Stanton,[1,2] a variety of structures have been diagnosed as suffering from ASR, from dams and nuclear power plant structures to bridges and parking structures. The Sixth Street Viaduct in Los Angeles, CA,[3] and several highway bridges in the Netherlands[4] and Denmark,[5] for example, have been demolished due to extensive ASR-induced damage that led to structural safety concerns.

The effect of ASR on structural behavior is comprised of a series of mechanisms which make conventional linear-elastic analyses inadequate.[6] The induced expansion, strongly influenced by internal and external restraints and sustained long-term loading, is usually accompanied by degradations in the mechanical properties of the concrete. As the reaction develops within a reinforced concrete element, the reinforcement acts as an internal restraint against the expansion, developing tensile stresses and thus inducing compressive stresses in concrete. Structural concrete is usually subjected to different stress levels in the principal directions, leading to anisotropic expansions and possibly anisotropic mechanical properties. Another mechanism with a notable effect on structural behavior is concrete strength enhancement due to confinement arising from prestressing of the reinforcement. Other factors with a potentially significant influence are degraded bond strength, reinforcement buckling, and cover spalling. In addition, the ASR-induced cracking is most likely to have serious consequences on the long-term durability of reactive structures.

A survey of the literature found results showing both increases and decreases in the capacity of ASR-affected shear-critical specimens when compared to similar non-reactive specimens or to theoretical strength. Shown in Table 1 is a summary of the test specimens reported in the literature. For each experimental program, the mean and coefficient of variation (COV) of the ratio between the load capacity of the reactive specimens and that of the non-reactive control ones ($P_{ASR}/P_{Control}$) is given, as is the level of linear unrestrained expansion measured ($\varepsilon_{ASR.free}$). For the tests on specimens extracted from existing ASR-affected structures, the ratio of experimental-to-calculated ultimate load is presented. Note that the calculated ultimate loads as reported by the researchers performing the tests did not include the ASR prestressing effect. Significant variability is seen with the mean of $P_{ASR}/P_{Control}$ ranging between 0.77 and 1.91.

RESEARCH SIGNIFICANCE

Contradicting experimental results were reported in the literature concerning the effects of ASR on the structural performance of shear-critical reinforced concrete elements. The tests performed in this work investigate the response of reinforced concrete panels cast with different types of reactive aggregate, different reinforcement ratios, experiencing

ACI Structural Journal, V. 118, No. 4, July 2021.

MS No. S-2020-335.R1, doi: 10.14359/51732651, received September 4, 2020, and reviewed under Institute publication policies.

Table 1—Summary of ASR-affected shear-critical specimens reported in literature

No. of specimens	Dimensions b x h x l, mm	$P_{ASR}/P_{Control}$ Mean	$P_{ASR}/P_{Control}$ COV, %	$\varepsilon_{ASR.free}$, × 10^{-3}	Additional observations
Bach et al.[7]—accelerated curing, monotonic loading, no vertical reinforcement					
13 beams	180 x 360 x 4300	1.77	25.8	7.3 to 11.1	Both increase and decrease measured
8 slabs	120 x 950 x 950	0.91	27.9	7.3 to 11.1	
Schmidt et al.[8]—in-place test, monotonic loading, no vertical reinforcement					
1 slab strip	1000 x 270* x 950	1.91†	—	—	Calculated load without ASR prestressing effect
Barbosa et al.[9]—monotonic tests on beams with no vertical reinforcement sawn from bridge					
10 slab strips	410‡ x 300 x 2600§	1.33‖	15.2	—	Calculated load without ASR prestressing effect
den Uijl and Kaptijn[4]—monotonic tests on beams with no vertical reinforcement sawn from bridge					
8 slab strips	480# x 600** x 7500††	0.77†	7.0	—	Calculated load without ASR prestressing effect
Ng and Clark[10]—accelerated curing, monotonic tests on slabs with no vertical reinforcement					
20 slabs	80 x 610 x 610	1.08	35.5	1.3 to 5.8	Both increase and decrease measured
30 slabs	80 x 460 x 460	0.99	13.9	0.2 to 7.9	Both increase and decrease measured
Clayton et al.[11]—accelerated curing, monotonic tests on I-beams					
4 beams	200 x 400 x 2500	0.78	5.7	1.0	Prestressed beams with vertical reinforcement
4 beams	200 x 400 x 2500	0.97	3.7	4.0	
4 beams	120 x 240 x 2500	0.80	0.0	1.0	Regular beams, no vertical reinforcement
4 beams	200 x 400 x 2500	0.78	7.1	4.0	
Ahmed et al.[12]—accelerated curing, monotonic and fatigue tests					
3 beams	80 x 130 x 1300	1.10	1.7	1.7 to 2.7	Monotonic loading
4 beams	80 x 130 x 1300	1.10	1.6	1.7 to 2.7	Fatigue loading
Deschenes et al.[13]—outdoor curing, beams with vertical reinforcement					
2 beams	533 x 1067 x 8433	0.95	2.76	1.7 to 4.5	a/d = 1.85
2 beams	533 x 1067 x 8433	1.25	2.41	1.9 to 6.9	a/d = 3.0
Habibi et al.[14]—accelerated curing, shear wall specimens, reversed cyclic loading					
3 shear walls	100 x 750 x 1300	1.08	4.47	1.9 to 2.2	ASR walls had reduced ductility

*Varying thickness 270 to 450 mm.

†Ratio of exp.-to-calc. ultimate loads.

‡Varying width 410 to 450 mm.

§Varying length 2600 to 3700 mm.

‖Ratio of exp.-to-calc. shear stress ($\tau = V/bd$).

#Varying width 480 to 570 mm.

**Varying thickness 650 to 750 mm.

††Varying length 7500 to 8500 mm.

Note: P_{ASR} represents the capacity of the reactive specimens and $P_{Control}$ represents the capacity of the non-reactive control ones. 1 mm = 0.0394 in.

different levels of ASR-induced damage, tested under in-plane pure shear loading conditions. The results provide additional insight into the counteracting and simultaneously occurring mechanisms that develop within ASR-affected shear-critical structures.

EXPERIMENTAL PROGRAM

Specimen description

To improve understanding of ASR effects on the response of ASR-affected reinforced concrete elements, a comprehensive experimental investigation was undertaken involving panel specimens loaded in pure membrane shear. The specimens were nominally identical, 890 mm (35.6 in.) square x 70 mm (2.8 in.) thick, cast with non-reactive, reactive fine (Jobe-Newman), or reactive coarse (Spratt) aggregate.

The concrete mixture design (Table 2) was based on the proportions suggested in ASTM C1293[15] with slight adjustments made according to the results of trial batches. The concrete from the initial trials had reduced workability and an average 28-day compressive strength of 52 MPa (7500 psi). Thus, for this study, the grading of the coarse aggregate and the water-cement ratio (w/c) were modified to

Table 2—Concrete mixture design

	ASTM C1293	Current mixture
Cement, kg/m^3	420	410
Water, kg/m^3	185	205
Fine aggregate, kg/m^3	721	730
Coarse aggregate, kg/m^3	1113	1000
w/*c*	0.42	0.50
Unit weight, kg/m^3	2440	2345
28-day strength, MPa	52	42

Note: 1 kg/m^3 = 0.062 lb/ft^3; 1 MPa = 145 psi.

Table 3—Chemical composition of general use cement

	%
LOI	1.93
SiO_2	19.05
Al_2O_3	5.12
Fe_2O_3	2.46
CaO	62.52
MgO	2.47
SO_3	4.05
Free lime	1.375
Na_2O_{eq}	0.96

Note: LOI is loss on ignition.

increase the workability of the fresh concrete. The maximum aggregate size was limited to 9.5 mm (0.37 in.), compared to 19.0 mm (0.75 in.) in the standard mixture design, and the *w*/*c* was increased to 0.50.

The control mixture contained non-reactive fine and coarse aggregate, obtained from a local source. Two reactive mixtures were investigated: one containing reactive coarse aggregate and non-reactive fine aggregate; and the other one containing reactive fine aggregate and non-reactive coarse aggregate. The reactive coarse aggregate was Spratt aggregate from Stittsville, ON, Canada, supplied by the Ministry of Transportation of Ontario. Spratt aggregate is slightly siliceous, with 9% SiO_2, and meets the physical requirements for concrete aggregate.[16] It has been extensively used by researchers for studying ASR expansion.[14,17-19] The reactive fine aggregate was Jobe-Newman sand from El Paso, TX, provided by the University of Texas at Austin. The sand was found to be highly reactive for both laboratory conditions and field exposure.[13]

General use cement with a total alkali content of 0.96% Na_2O equivalent by mass of cement was used for all casts. The chemical composition of the cement is shown in Table 3. The alkali content was supplemented for the reactive mixtures by adding sodium hydroxide (NaOH) to reach a total of 1.25% Na_2O equivalent by mass of cement. The non-reactive cast did not have the alkali content boosted.

Each cast produced two panels, three ASTM C1293 expansion prisms, and nine standard 100 mm (4 in.) Φ cylinders. The specimens were moist-cured for a total of 72 hours, after which they were stored at ambient temperature, approximately 21°C, until the accelerated conditioning process started.

Table 4—Panel specimen test matrix

ID	ρ_x, %	ρ_y, %	ρ_z, %	Reactive aggregate	Loading protocol
AF1	3.31	0.42	—	None	Monotonic
AF2	3.31	0.84	—		
AF3	3.31	0.42	—	Jobe-Newman	Monotonic
AF4	3.31	0.84	—		
AF5	3.31	0.42	—	Spratt	Monotonic
AF6	3.31	0.84	—		
AF7	3.31	0.42	1.69	Jobe-Newman	Monotonic
AF8	3.31	0.84	1.69		
AF9	3.31	0.20	—	Jobe-Newman	Monotonic
AF10	3.31	1.66	—		Cyclic

The panel specimen test matrix, shown in Table 4, summarizes the reinforcement ratios provided in-plane (X-, Y-directions) and out-of-plane (Z-direction), ρ_x, ρ_y, and ρ_z, the reactive aggregate used in the mixture, and the loading protocol. For all panels, 40-D8 deformed bars were used in the X-direction, giving a reinforcement ratio of 3.31%. In the Y-direction, the reinforcement ratio varied from 1.66% provided by 20-D8 bars, to 0.84% provided by 20-D4 deformed bars, to 0.42% provided by 10-D4 deformed bars, to 0.20% provided by 10-8/32 in. threaded rods. Along the Y-direction, the edges of the panels were reinforced with short 5/16 in. (8 mm) threaded rods to assist the load transfer from the shear keys to the reinforced concrete panel and to avoid localized edge failure due to stress concentration. Figure 1 shows the two typical reinforcement configurations used, and Fig. 2 presents a view of a test specimen containing out-of-plane reinforcement before the cast.

The shear keys, cast around the perimeter of a panel specimen, were removed 72 hours after casting to reuse them for subsequent casts. The inside surfaces of the shear keys were spray-painted with a rubber-based film to prevent damage to the concrete during the removal procedure. The reinforcement bars that remained exposed were spray-painted with three layers of paint to prevent rust. The rust protection was reapplied twice during the conditioning period due to high humidity damage.

Accelerated conditioning and expansion measurement

The specimens were placed inside an environmentally controlled chamber to accelerate the reaction. At the time the accelerated conditioning protocol started, the ages of the specimens were 563 days for Panels AF1 and AF2, 547 days for AF3 and AF4, 477 days for AF5 and AF6, 519 days for Panels AF7 and AF8, and 463 days for Panels AF9 and AF10. The panel specimens were stored vertically on a steel support, with sufficient space between them to allow uniform moisture ingress. The panels and the accompanying

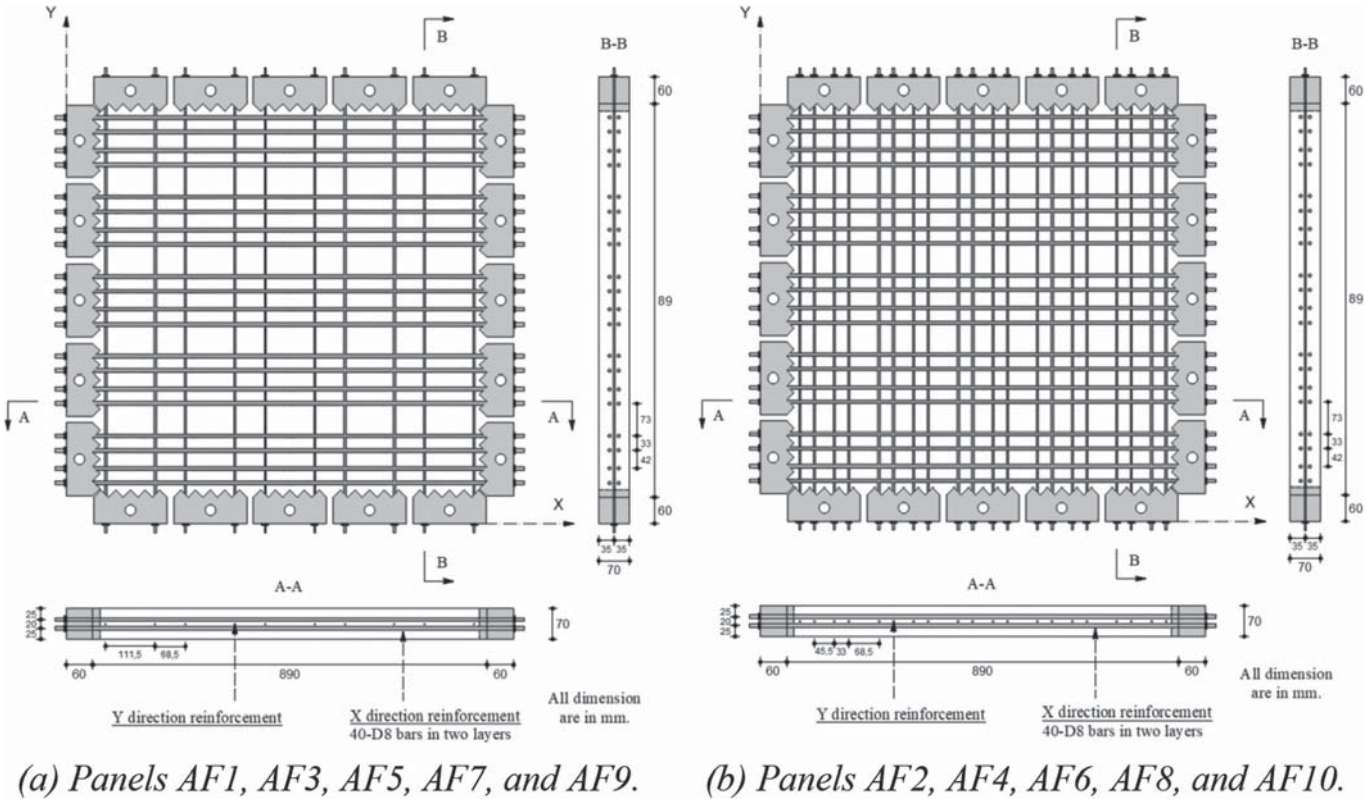

(a) Panels AF1, AF3, AF5, AF7, and AF9. (b) Panels AF2, AF4, AF6, AF8, and AF10.

Fig. 1—Typical reinforcement configuration. (Note: 1 mm = 0.0394 in.)

Fig. 2—Panel AF8 before casting.

specimens were maintained at a temperature of 50 ± 0.5°C, and in 97 ± 3% relative humidity.

Expansion measurements were taken periodically to monitor the unrestrained longitudinal strains of the ASTM C1293 prisms. Shown in Fig. 3(a) is the expansion evolution during the conditioning period as measured from prisms corresponding to each cast. All reactive casts exceeded the threshold for reactivity specified by ASTM C1293 (0.40×10^{-3}), while the non-reactive cast remained below it, measuring 0.12×10^{-3} before the tests. The ASR-induced expansion measured for Cast 3, containing reactive Spratt coarse aggregate, reached exhaustion after approximately 150 days in the accelerated conditioning environment. At the end of the conditioning period the average strain measured on the prisms was equal to 1.23×10^{-3}. The Jobe-Newman casts all reached higher levels of expansion. The trend of the expansion was also different. Between 50 and 70 days, the Jobe-Newman casts showed a significantly increased expansion rate compared to the Spratt cast. Moreover, the exhaustion level was reached later for the Jobe-Newman casts, after approximately 180 days in the accelerated conditioning environment. At the end of the conditioning period, the expansion levels were 2.32×10^{-3} for Cast 2, 2.50×10^{-3} for Cast 4, and 2.36×10^{-3} for Cast 5.

In addition, strain measurements on the panels' surfaces were taken from Zurich targets applied over a gauge length of 200 mm along X- and Y-directions in the central region of the specimen. For the specimens that were part of Cast 3, Fig. 3(b) shows the surface strain measurements on the panels versus the prism strains. Anisotropic strains were developed as a result of different reinforcement ratios. At the end of the conditioning period, both Panels AF3 and AF4 had similar strains along the X-direction (3.31% reinforcement ratio): 0.94×10^{-3} for AF3 and 0.87×10^{-3} for AF4. The strain in the Y-direction of Panel AF3 (0.42% reinforcement ratio) was equal to 2.22×10^{-3}, nearly matching the strain measured on the unrestrained expansion prisms (2.32×10^{-3}). However, the trend of the expansion was different, with strain discrepancies between the Y-direction and the unrestrained prisms between 70 and 150 days. In this interval, the prisms underwent a gradual expansion, while the panel surface strains remained constant. The difference in strain measurement was significantly reduced once the first observable cracks developed.

The Y-direction of Panel AF4 had a 0.84% reinforcement ratio and, at the end of the conditioning period, the expansion measured 1.56×10^{-3} (Fig. 3(b)). The expansion trend was similar to the one observed in the Y-direction for Panel AF3. Comparing the strains along the Y-direction of Panels AF3 and AF4, it can be seen that decreasing the reinforcement

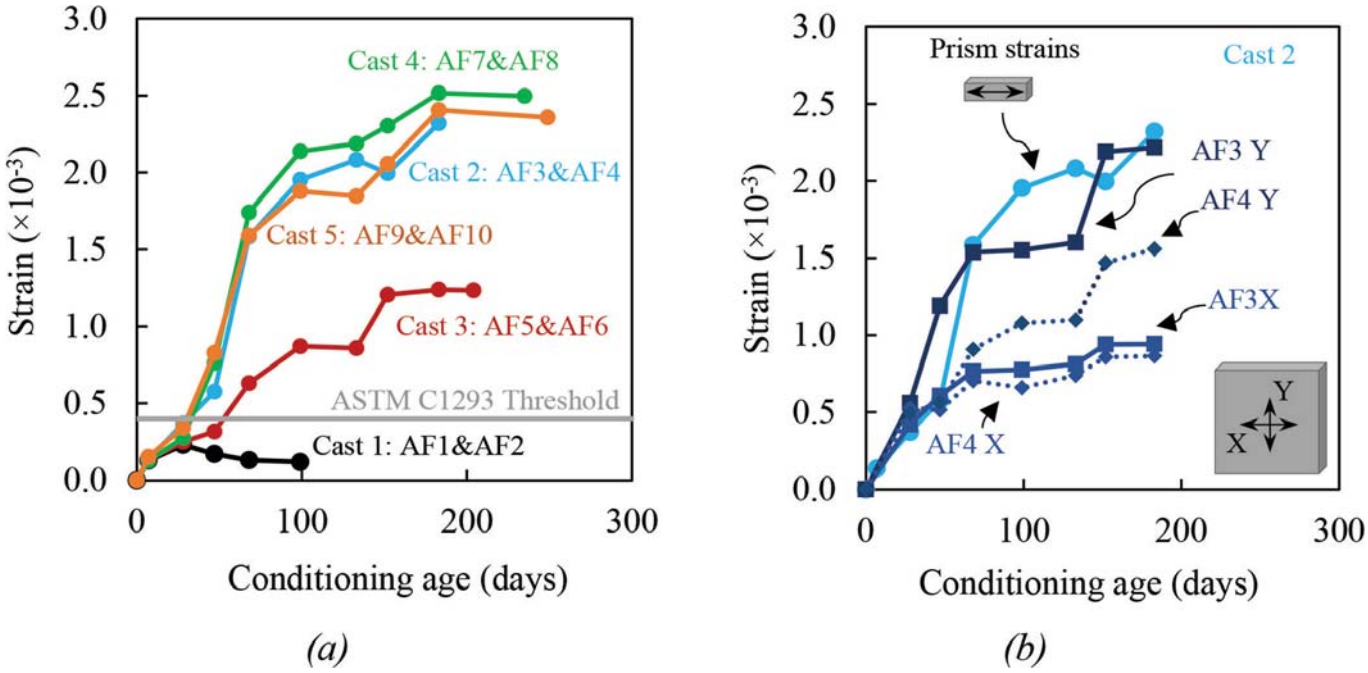

Fig. 3—ASR-induced expansion: (a) ASTM C1293 prisms strains; and (b) Panels AF3 and AF4 surface strains versus corresponding prism strains.

ratio from 0.84 to 0.42% resulted in an increase of 42% in the ASR-induced expansion along the direction of the reinforcement.

Similar strain measurements performed for the rest of the specimens indicated that along a given direction, reinforcement ratios of 0.42% or lower did not do much to restrain ASR expansion. Conversely, reinforcement ratios of 1.66% and 3.31% had similar strong restraining influences on the expansion, preventing the formation of ASR-induced cracks in their direction.

Test setup, instrumentation, and data acquisition

The panel specimens were tested under in-plane pure shear loading conditions using the Panel Element Tester (Fig. 4), designed and developed at the University of Toronto[20] to apply combinations of shear and tension or compression on 890 mm (35 in.) square x 70 mm (2.76 in.) thick specimens. It was the first such testing equipment capable of applying pure shear stresses on large reinforced concrete elements. The Modified Compression Field Theory,[21] which is the basis for the shear design provisions in the Canadian, Australian, Eurocode, and AASHTO design standards, was developed based on experimental results obtained using the Panel Element Tester.

The loading on a concrete test panel was applied around its perimeter through 20 shear keys. Each shear key was connected to two links at 45 degrees to each side of the normal to the edge of the panel. To produce pure shear, one link had to apply a tension force and the other link had to apply an equal compression force. The forces in the links were supplied by 37 double-acting hydraulic jacks and three rigid links that stabilized the panel element within the testing rig. A load maintainer was used to produce, from a single constant input hydraulic pressure, the two separate variable output hydraulic pressures required. One pressure (0.438P)

Fig. 4—Panel specimen in Panel Element Tester.

was used for the advancing jacks and the other pressure (P) for the retracting jacks. This was required for the same force to be applied in both directions, as a hydraulic cylinder has different advancing and retracting areas. Out-of-plane translations were resisted by a lateral support frame, bolted to the main reaction frame, connected to the shear keys by tie rods with spherical bearings that permitted free in-plane movement but restricted out-of-plane movement.

The panel specimens were instrumented to record states of strain and stress during the test. An in-house analogue data acquisition system was used to store data from the linear variable differential transducers (LVDTs), load cells, and pressure transducers simultaneously. The system was programmed to save data when the pump pressure changed by 30 psi, equivalent to 0.033 MPa (4.78 psi) applied shear stress, or the horizontal/vertical LVDTs measurements

Table 5—Reinforcement properties

ID	E_s, GPa	f_y, MPa	ε_y, × 10^{-3}	f_{sh}, MPa	ε_{sh}, × 10^{-3}	f_u, MPa	ε_u, × 10^{-3}
D8	194.9	543	2.79	554	4.85	584	27.4
D4	187.1	603	3.23	615	5.29	633	17.6
8/32	177.8	645	3.66	643	6.08	740	34.0

Note: 1 GPa = 145 ksi; 1 MPa = 145 psi.

changed by 0.10 mm (3.97 × 10^{-3} in.), equivalent to 0.10 × 10^{-3} strain. Additionally, photographs and video were taken throughout the tests.

The strain state was obtained from measurements taken by the LVDTs. During a test, on each face of the panel, six LVDTs measured the displacements between two fixed points along four directions. On each face, one LVDT was placed vertically, one horizontally, two in the X-direction, and two in the Y-direction. The average strain in each direction was calculated by dividing the LVDT displacements by the original gauge length. Thus, using a Mohr's Circle approach, the strain in any direction could be derived. The assumption was made that the LVDT rods remained rigid; there was no indication during the tests that this assumption was not valid.

The hydraulic pressures in the system were recorded by four pressure transducers. Two of the transducers were positioned at the upstream ends of the two different input pressure lines, and the other two were set up at the downstream ends of the lines to monitor any potential inconsistency. With the actuators each having been individually force-pressure calibrated, the applied stresses on the panels could be determined from the pressure measurements.

EXPERIMENTAL RESULTS

This section presents the experimental shear load-deformation responses of the 10 panel specimens, along with other selected data and observations. More comprehensive test results and analyses are presented elsewhere.[22]

ASR-induced prestress

For the reactive panel specimens, the ASR-induced prestresses were determined employing compatibility and equilibrium conditions together with the Zurich measurements and the reinforcement coupon stress-strain data (Table 5). From compatibility conditions, the average strains of the reinforcement were considered to be equal to the total average strains of the panel, determined prior to the shear test from Zurich target measurements. Next, the reinforcement stresses were determined using the Ramberg-Osgood function[23,24] presented in Appendix A.1.* Finally, the average concrete stresses were calculated from equilibrium conditions. The procedure for calculating the panel stresses and strains is detailed in Appendix A.2.

The concrete and reinforcement stresses in the X- and Y-directions, f_{cx}, f_{cy}, f_{sx}, and f_{sy}, are shown in Table 6 for all reactive panel specimens prior to testing. The magnitude of the initial stress state was influenced by the reinforcement ratio and the reactivity of the concrete mixture, and it directly influenced the behavior of the panels during the shear tests.

Table 6—Reactive panels: concrete and reinforcement stress state before testing

ID	f_{cx}, MPa	f_{cy}, MPa	f_{sx}, MPa	f_{sy}, MPa
AF3	–6.06	–1.74	183	414
AF4	–5.55	–2.45	168	292
AF5	–3.74	–0.98	113	234
AF6	–4.78	–1.74	144	208
AF7	–2.84	–1.11	86	264
AF8	–3.74	–2.12	113	252
AF9	–5.68	–0.89	171	444
AF10	–5.23	–3.33	158	201

Note: 1 MPa = 145 psi.

Test observations

A summary of the experimental data is presented in Table 7 for all panel specimens in terms of: concrete compressive strength at test day, f_{cp}; concrete modulus of elasticity, E_c; ASR-induced surface strains, $\varepsilon_{x.ASR}$ and $\varepsilon_{y.ASR}$; ASR free strains measured from corresponding expansion prisms, ε_{ASR}; shear stress at first cracking, ν_{cr}; shear strain at first cracking, γ_{cr}; ultimate shear stress, ν_u; and ultimate shear strain, γ_u.

The reported concrete compressive strengths and moduli of elasticity at test day are the averages of three compressive tests on standard 100 mm (4 in.) Φ x 200 mm (8 in.) cylinders. The cylinders' compressive stress-strain responses are presented in Appendix A.3. For the reactive concrete mixtures, a substantial reduction in the moduli of elasticity was observed compared to the non-reactive one, while the concrete compressive strengths were not affected to the same extent.

The shear stress at cracking, ν_{cr}, and the shear strain at cracking, γ_{cr}, are reported for the moment when the first visible shear crack developed during the test due to the applied loading (Table 7). For all panels, concrete cracking produced a noticeable change in the stiffness of the response. The reactive panels cracked at higher applied shear stresses compared to the non-reactive panels due to the ASR-induced prestress.

The ultimate shear stress capacities of the reactive panels were marginally higher compared to the corresponding non-reactive panels; however, the deformation capacities were reduced by roughly 30%. Across the reactive panels, those containing the same reinforcement ratios exhibited

*The Appendix is available at **www.concrete.org/publications** in PDF format, appended to the online version of the published paper. It is also available in hard copy from ACI headquarters for a fee equal to the cost of reproduction plus handling at the time of the request.

Table 7—Summary of panel tests

ID	f_{cp}, MPa	E_c, MPa	$\varepsilon_{x.ASR}$, × 10^{-3} $\varepsilon_{y.ASR}$, × 10^{-3} ε_{ASR}, × 10^{-3}	v_{cr}, MPa	γ_{cr}, × 10^{-3}	v_u, MPa	γ_u, × 10^{-3}
AF1	57.2	33,700	0.35* 0.35* 0.12*	2.19	0.24	6.75	9.59
AF2	58.4	33,500	0.35* 0.27* 0.12*	2.74	0.32	8.64†	6.54†
AF3	38.2	18,300	0.94 2.22 2.32	4.34	0.53	6.99	6.50
AF4	41.3	18,600	0.86 1.56 2.32	4.32	0.35	9.77	7.37
AF5	52.5	21,000	0.58 1.25 1.23	3.96	0.33	6.99	6.67
AF6	52.1	20,100	0.74 1.11 1.23	4.32	0.49	9.63	7.39
AF7	46.3	21,200	0.44 1.41 2.49	4.90	0.50	7.33	7.07
AF8	47.1	19,400	0.58 1.35 2.49	5.67	0.87	10.42	7.83
AF9	46.9	18,900	0.88 2.50 2.36	3.90	0.25	4.79	3.81
AF10	50.9	21,200	0.81 1.03 2.36	5.21	0.48	10.79	5.98

*Expansion primarily attributed to swelling due to water absorption.

†Edge failure.

Note: 1 MPa = 145 psi.

virtually identical structural behavior, regardless of the ASR-induced expansion level. These results are indicative of counterbalancing ASR-induced mechanisms: beneficial prestressing effects offsetting material deterioration.

The higher cracking loads of the reactive specimens relative to those of the non-reactive ones, coupled with the fact that the ultimate load capacities were little changed, meant that the margins between cracking and failure in terms of both strength and deformation capacity were significantly reduced due to ASR. This can potentially have significant implications for the reserve capacity of ASR-affected structures from the moment the first signs of distress are visible to structural failure.

For panels containing 0.42% and 0.20% reinforcement in the Y-direction, failure was initiated by yielding of the reinforcement leading to aggregate interlock failure and subsequently to sliding along the crack surface. Figure 5(a) shows a typical crack pattern at failure representative for this failure mechanism. The panels which contained higher reinforcement ratios in the Y-direction, 0.84% and 1.66%, exhibited a more brittle failure mechanism, led by crushing of concrete after yielding of the Y-direction reinforcement (Fig. 5(b)). Appendix A.4 chronicles all panels' crack patterns and failure modes.

Discussion of experimental results

Lightly reinforced panels—Shown in Fig. 6 is a comparison between the experimental shear stress-shear strain responses of Panels AF1, AF3, AF5, and AF7. All of these panels contained 3.31% X-direction reinforcement and 0.42% Y-direction reinforcement. Panel AF7 also had 1.69% out-of-plane reinforcement. Specimen AF1 was the control specimen, cast with non-reactive concrete; Panels AF3 and AF7 were cast with the highly-reactive Jobe-Newman fine aggregate; and Panel AF5 was cast with reactive Spratt coarse aggregate. Therefore, a direct comparison can be made of the behavior of specimens cast with different types of reactive aggregates, which underwent different levels of expansion and that contained the same amounts of in-plane reinforcement.

Reactive Panels AF3 (Jobe-Newman) and AF5 (Spratt) had virtually identical responses in terms of pre-cracking and post-cracking stiffness, and shear stress and shear strain values at failure, despite differences in concrete compression

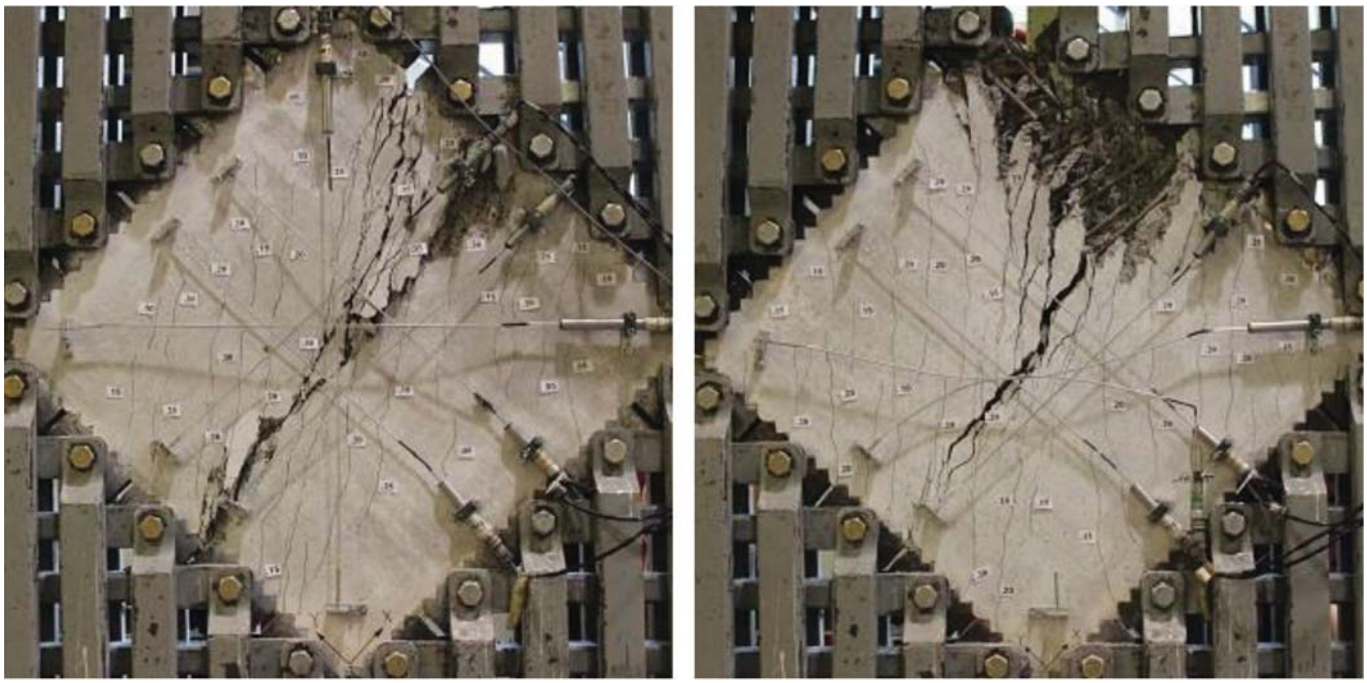

(a) Panel AF5. (b) Panel AF6.

Fig. 5—Typical crack patterns at failure.

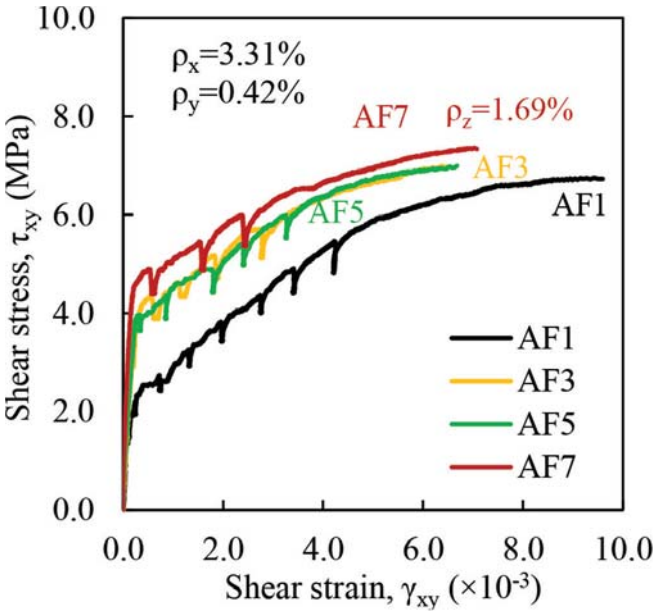

Fig. 6—Shear stress-strain responses of lightly reinforced panels AF1, AF3, AF5, and AF7. (Note: 1 MPa = 145 psi.)

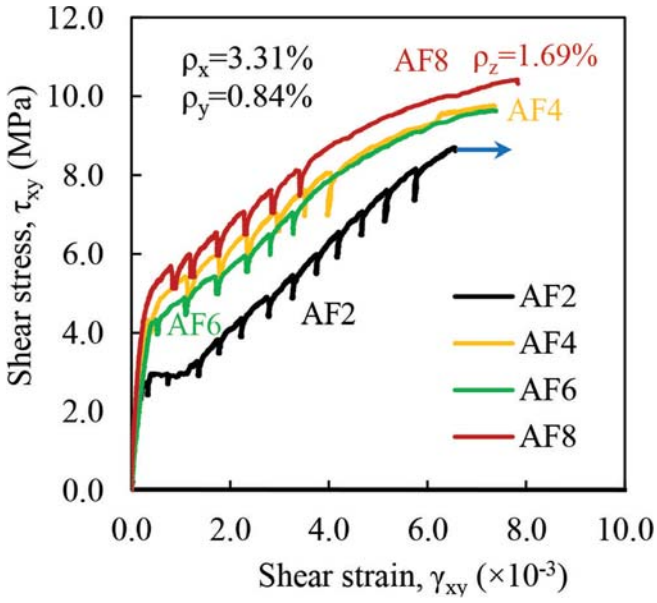

Fig. 7—Shear stress-strain responses of highly reinforced panels AF2, AF4, AF6, and AF8. (Note: 1 MPa = 145 psi.)

strength and notable differences in the ASR-expansion levels (Table 7). Another significant difference was the fact that Panel AF5 presented no visual ASR-induced cracks that would have indicated the occurrence of a deleterious mechanism within the concrete.

Compared to control Panel AF1, reactive Panels AF3 and AF5 sustained marginally higher shear stresses at failure. The differences in shear strain at failure, however, were pronounced as the reactive panels at failure only reached on average 68% of the ultimate shear strain of the control panel. Another significant difference between the reactive panels and the control panel was the cracking stress. Due to the biaxial compression state the reactive concrete was experiencing, the load-induced cracks in the ASR specimens first developed at shear stress levels that were nearly double those of Panel AF1. Therefore, as previously mentioned, for the reactive panels, the load margin between the development of the first visible load-induced cracks and failure was substantially reduced.

Panel AF7 had a slightly better performance compared to reactive panel AF3. Both panels were cast with the same type of reactive aggregate and contained the same amount of in-plane reinforcement. A comparison between their responses highlights the influence of the out-of-plane

reinforcement. Panel AF7 exhibited a 5% increase in the ultimate shear stress and a 9% increase in the ultimate shear strain. The cracking shear stress was also higher for Panel AF7, showing a 13% increase. This slightly enhanced performance was attributed to the out-of-plane confinement stresses experienced by the concrete in Panel AF7.

Highly reinforced panels—Figure 7 shows the experimental shear stress-shear strain responses of the highly reinforced panel specimens AF2, AF4, AF6, and AF8. The panels all contained 3.31% X-direction reinforcement and 0.84% Y-direction reinforcement. In addition, Panel AF8 had 1.69% out-of-plane reinforcement. Panel AF2 was the control specimen, cast with non-reactive concrete, Panels AF4 and AF8 were cast with the highly reactive Jobe-Newman fine reactive aggregate, and Panel AF6 was cast with the reactive Spratt coarse aggregate. Therefore, similar to the previous discussion for the lightly reinforced panels, a comparison can be made for the behavior of specimens cast with different types of reactive aggregates, which underwent different levels of expansion, but contained the same amounts of in-plane reinforcement. The major trends that emerge from a comparison of the highly reinforced panels are similar to those observed from the lightly reinforced panels.

Panels AF4 and AF6 had similar responses despite different concrete compressive strengths and ASR expansion levels (Table 7). Thus, in this study, the counterbalancing effects of ASR-induced material deterioration and prestressing due to restrained expansion were equivalent for the panels with 0.84% Y-direction reinforcement (AF4 and AF6) and the panels with 0.42% Y-direction reinforcement (AF3 and AF5).

The disparities in the responses of reactive Panels AF4 and AF6 with respect to control Panel AF2 were similar to the disparities observed for the lightly reinforced panels. The shear stress that produced the first load-induced cracking was 57% higher for the reactive panels compared to the non-reactive specimen, attributable to the initial biaxial compression state of the reactive concrete.

A comparison of the ultimate shear stress and strain values has to be made, recognizing the fact that control specimen AF2 had a slightly premature failure caused by a shear key pullout as the reinforcement ruptured at a threaded section inside the key. This failure occurred after the Y-direction reinforcement started yielding. Thus, based on the behavior of the other panels tested, it is assumed that the ultimate shear stress measured was close to the actual capacity of the panel. The measured shear strain, on the other hand, is not considered to be representative of the deformation capacity of the panel as it most likely would have been higher had an edge failure not occurred. In terms of shear stress at failure, the reactive panels showed an increase of 13% for AF4 and 11% for AF6.

Panel AF8 exhibited slightly improved behavior in terms of ultimate shear stress and shear strain capacities compared to Panel AF4, owing to the out-of-plane concrete compressive stresses which developed due the presence of the Z-direction reinforcement. The increases in strength and ductility were in the same range as the increases measured

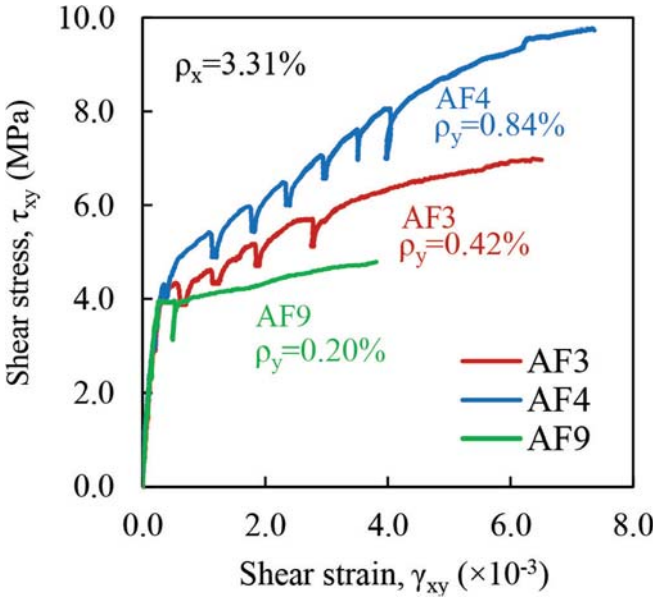

Fig. 8—Shear stress-strain responses of Panels AF3, AF4, and AF9. (Note: 1 MPa = 145 psi.)

for the lightly reinforced panels: 6% increases in both shear strength and ultimate shear strain.

Influence of Y-direction reinforcement ratio—Panels AF3, AF4, and AF9 were cast with the same amount of X-direction reinforcement and the same type of reactive aggregate, but with different amounts of Y-direction reinforcement (Table 4). Figure 8 compares their experimental shear stress-shear strain responses.

The panels developed ASR-induced cracks that were 80 mm (3.15 in.) apart, oriented parallel to the X-axis, as shown in Appendix A.4. The average crack widths were 0.20, 0.05, and 0.10 mm (7.87×10^{-3}, 1.97×10^{-3}, and 3.97×10^{-3} in.), for Panels AF3, AF4, and AF9, respectively. The ASR-induced cracks increased slightly in width until the formation of cracks caused by the shear loading.

For Panel AF9, the ASR-induced average crack width measured 0.15 mm (5.91×10^{-3} in.), at a shear stress of 3.78 MPa (550 psi) and a shear strain of 0.24×10^{-3}; the spacing remained unchanged. This initial load stage was taken immediately before the panel developed a crack due to the applied loading, oriented at 30 degrees to the X-axis. As the panel was nearing failure, several other cracks developed, giving a crack spacing of approximately 160 mm (6.30 in.). The failure plane developed along the interfaces of the first crack, which showed no change in orientation as the load increased. Shown in Appendix A.4 is the crack pattern at failure.

As shown in Fig. 8, the pre-cracking stiffnesses of Panels AF3, AF4, and AF9 were virtually identical; moreover, the cracking strengths were also similar. Post-cracking stiffnesses diverged significantly, however, reflective of the reinforcement ratios in the Y-direction: the higher the reinforcement ratio, the stiffer the post-cracking response.

In terms of ultimate shear stress, Panels AF9, AF3, and AF4 reached 4.79, 6.99, and 9.77 MPa (695, 1014, and 1417 psi), respectively. As such, the cracking loads represented 81%, 62%, and 44% of the ultimate loads for

Table 8—Concrete principal tensile stresses at cracking

ID	$f_{c1.cr}$, MPa	$f_{t.ACI}$, MPa	$f_{c1.cr}/f_{t.ACI}$
AF1	2.00	2.50	0.80
AF2	2.48	2.52	0.98
AF3	0.82	2.04	0.40
AF4	0.53	2.12	0.25
AF5	1.80	2.39	0.75
AF6	1.19	2.38	0.50
AF7	2.72	2.25	1.21
AF8	2.31	2.26	1.02
AF9	1.26	2.26	0.56
AF10	0.67	2.35	0.28

Note: 1 MPa = 145 psi.

Panels AF9, AF3, and AF4. It can be concluded that the reserve capacity after cracking reduced significantly with the reduction in the reinforcement ratio provided.

Cyclic shear test—Cast with reactive Jobe-Newman fine aggregate, Panel AF10 was tested under cyclic shear loading, with each cycle reaching a peak shear stress of 10.8 MPa (1600 psi). Shown in Fig. 9 is the experimental response of Panel AF10; crack patterns are presented in Appendix A.4. When the target shear stress of 10.8 MPa (1600 psi) was reached in the first loading cycle, the maximum crack width measured 0.35 mm (0.014 in.), the average crack width was 0.24 mm (0.009 in.), and the average crack spacing was 80 mm (3.15 in.). Yielding of the Y-direction reinforcement was reached during the third cycle of loading, at a shear stress of 10.6 MPa (1500 psi) and a shear strain of 4.81×10^{-3}. The last load stage taken was after 14 cycles, when the maximum crack width measured 0.55 mm (0.02 in.), the average crack width was 0.35 mm (0.014 in.), and the average crack spacing was 80 mm (3.15 in.). Failure occurred during the 15th cycle of loading due to concrete crushing, at a shear stress of 10.8 MPa (1600 psi) and a corresponding shear strain of 5.98×10^{-3}.

Concrete principal tensile stresses at cracking—With the exception of the panels containing out-of-plane reinforcement, the concrete principal tensile stresses at cracking, $f_{c1.cr}$, were significantly lower for the reactive panels, compared to the non-reactive ones and to ACI 318-calculated tensile strengths, $f_{t.'ACI}$ (Eq. (1))

$$f'_{t.ACI} = 0.33\sqrt{f'_c} \quad (\text{MPa})$$
$$f'_{t.ACI} = 4.0\sqrt{f'_c} \quad (\text{psi}) \tag{1}$$

The experimental concrete principal stresses were determined as described in Appendix A.2. The values of the concrete principal tensile stresses at cracking are summarized in Table 8 along with the code-based tensile strengths. As the concrete compressive strengths did not vary significantly for the panels tested (Table 7), neither did the computed tensile strengths, $f_{t.'ACI}$, with values ranging from 2.04 to 2.52 MPa (296 to 365 psi). On the other hand, the concrete principal tensile stress at cracking measured during the tests varied

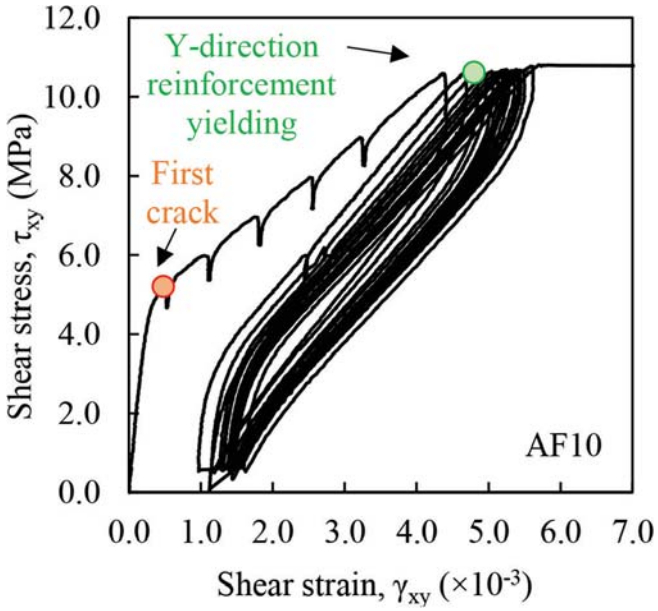

Fig. 9—Shear stress-strain response of Panel AF10—cyclic shear protocol. (Note: 1 MPa = 145 psi.)

significantly with values between 0.53 and 2.72 MPa (77 and 395 psi). In general, however, the significantly reduced cracking strength is reflective of ASR-induced deterioration in the mechanical tensile strength of concrete.

The highest discrepancies between ACI 318[25] values for the tensile strength and the measured tensile stress at cracking occurred for Panels AF4 and AF10. One potential contributing factor, besides the reduction in tensile strength, is that the reactive panels developed cracks parallel to the Y-direction. The shear load-induced cracks subsequently formed at an inclination of approximately 45 degrees to the X-axis, bridging the already existing cracks. During the tests, it was observed that these two systems of cracks were connected—the load-induced cracks were aligned at multiple locations with the ASR-induced ones.

At the other end of the spectrum are Panels AF7 and AF8, which contained out-of-plane reinforcement. These panels exhibited tensile concrete stresses at cracking somewhat higher than the tensile strengths calculated based on ACI 318. The out-of-plane compressive stresses improved the in-plane response of ASR-affected concrete, increasing the principal tensile stresses at cracking, as well as the ultimate capacity.

Figure 10 compares the calculated concrete tensile strengths and the observed ultimate strengths. The ratio of the principal tensile concrete stress at cracking to the ACI 318-based concrete tensile strength, $f_{c1.cr}/f_{t.'ACI}$, is shown for all panels. The ratio of the ultimate shear stress measured on the reactive panels to that of the corresponding non-reactive panels, $v_{u.R}/v_{u.N}$, is given for Panels AF1 through AF8; Panel AF9 did not have a corresponding control panel, and Panel AF10 was subjected to reversed cyclic loading condition. It is clearly evident that while the concrete tensile strength was significantly reduced for reactive panels with no out-of-plane reinforcement, the panels' ultimate shear strength was not adversely affected. The counterbalancing effects of the ASR-induced mechanical properties

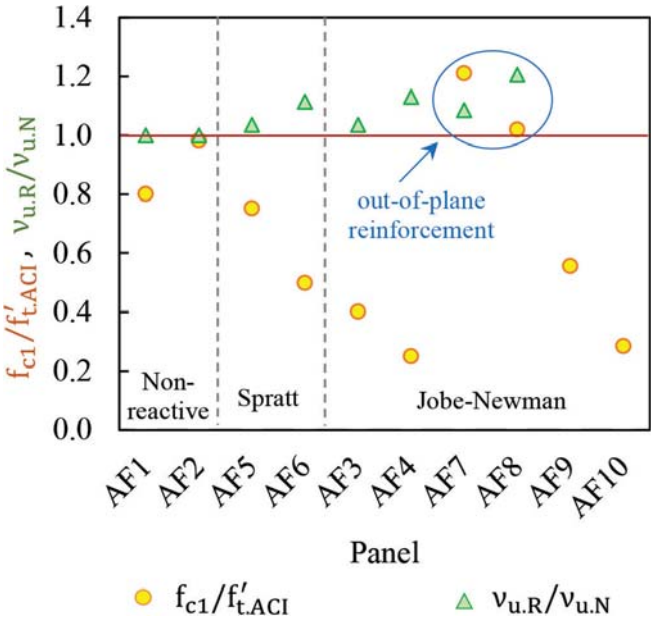

Fig. 10—Concrete principal tensile response versus ultimate strength.

deterioration and ASR-induced prestressing are particularly notable for Panels AF5 and AF6 (Spratt) and for Panels AF3 and AF4 (Jobe-Newman).

CONCLUSIONS

The experiments described herein represent a potentially significant contribution to the database of tests on ASR-affected shear-critical reinforced concrete elements, given the contradictory results previously reported in the literature. They are the first tests that investigate the behavior of ASR-affected reinforced concrete subjected to pure shear conditions. Moreover, the cyclic test adds to the limited body of literature on the cyclic deterioration of ASR-affected specimens.

For the range of conditions examined, the test results suggest the following conclusions:

1. The shear stress at cracking is higher for reactive elements, compared to non-reactive ones, due to the prestress induced in the concrete. The cracking strength can be increased by as much as 100% for elements with the same in-plane reinforcement ratio.

2. For reactive elements containing biaxial reinforcement, the concrete principal tensile stress at cracking is significantly lower compared to that of non-reactive elements. Moreover, the ACI 318 relationship for estimating tensile strength based on the compressive strength is dangerously unconservative. The experimental tensile strength can be as low as 25% of the estimated ACI 318 value.

3. The shear strength of orthogonally reinforced elements is not negatively impacted by ASR-induced deterioration, compared to similar non-reactive elements, regardless of the severity of the expansion.

4. A reduction in ductility is prevalent for ASR-reactive elements compared to similar non-reactive ones. However, the degree of ductility loss appears not affected by the level of ASR-induced expansion nor by the type of reactive aggregate used.

5. The orientation of shear cracks in reactive elements forms largely independently of the pre-existing ASR-induced cracks. The shear-induced cracks, however, propagate such that they bridge the already existing ASR cracks.

6. The eventual mode of failure in reactive elements, involving varying combinations of aggregate interlock loss and concrete compression failure depending on the reinforcement configuration, is not much different from that experienced by similarly reinforced non-reactive elements.

7. Reactive elements containing similar reinforcement ratios will exhibit similar responses whether they show signs of ASR deterioration (that is, cracking) prior to loading or not.

8. With ASR-reactive elements, the margin between cracking and failure is reduced in regard to both strength and deformation capacity. This can potentially have significant implications for ASR-affected structures in the field from the moment the first signs of distress are visible to structural failure.

9. Consistent with numerous results from the literature, the level of ASR-induced expansion is influenced by the long-term three-dimensional stress state of the element. Different in-plane strain conditions will develop in triaxially reinforced or restrained elements containing the same in-plane reinforcement ratios. Out-of-plane reinforcement reduces the expansion developed in the in-plane directions.

10. ASR is expected to compromise the long-term durability of concrete structures. Depending on the exposure conditions, ASR-induced cracking can accelerate mechanisms such as chemical attack and reinforcement corrosion.

It should be noted that these conclusions pertain to shear-critical elements containing at least minimum shear reinforcement, subjected to in-plane shear, and experiencing moderate levels of ASR expansion. They may not apply to elements containing no shear reinforcement, subjected to out-of-plane shear, or experiencing extreme levels of ASR expansion. Further research is required.

AUTHOR BIOS

Anca C. Ferche *is an Assistant Professor in the Department of Civil, Architectural and Environmental Engineering at the University of Texas at Austin, Austin, TX. She received her PhD from the University of Toronto, Toronto, ON, Canada, in 2020. Her research interests include performance assessment and analysis of reinforced concrete structures, concrete deterioration mechanisms, and rehabilitation of structures.*

Frank J. Vecchio, *FACI, is a Professor in the Department of Civil and Mineral Engineering at the University of Toronto. He received the following ACI awards: Structural Research Award (1998), Structural Engineering Award (1999), Wason Medal (2011), Joe Kelley Award (2016), and Arthur J. Boase Award (2020). His research interests include advanced constitutive modeling and analysis of reinforced concrete, assessment and rehabilitation of structures, and response to extreme loads.*

ACKNOWLEDGMENTS

The authors would like to acknowledge NSERC for funding support provided to this project. The authors would also like to acknowledge the Ontario Ministry of Transportation and the University of Texas at Austin for providing the reactive aggregate.

REFERENCES

1. Stanton, T. E., "California Experience with the Expansion of Concrete through Reaction between Cement and Aggregate," *ACI Journal Proceedings*, V. 38, 1942, pp. 209-215.

2. Stanton, T. E., "Expansion of Concrete through Reaction between Cement and Aggregate," *Proceedings American Society of Civil Engineers*, 1940, pp. 1781-1811. (Reprinted with discussion and closure in Transaction, ASCE, V. 107, pp. 54-126).

3. The Bureau of Engineering, "6th Street Viaduct Seismic Improvement Project," Los Angeles, CA, 2007, 5 pp.

4. den Uijl, J. A., and Kaptijn, N., "Shear Tests on Beams Cut from ASR-Affected Bridge Decks," *Large-Scale Structural Testing*, SP-211, American Concrete Institute, Farmington Hills, MI, 2003, pp. 115-134.

5. Hansen, S. G.; Barbosa, R. A.; Hoang, L. C.; and Hansen, K. K., "Shear Capacity of ASR Damaged Structures – In-Depth Analysis of Some in-situ Shear Tests on Bridge Slabs," *Proceedings of the 15th International Conference on Alkali-Aggregate Reaction in Concrete*, 2016.

6. CSA Special Publication A844-00, "Guide to the Evaluation and Management of Concrete Structures Affected by Alkali-Aggregate Reaction," CSA Group, Mississauga, ON, Canada, 2000.

7. Bach, F.; Thorsen, T. S.; and Nielsen, M. P., "Load-Carrying Capacity of Structural Members Subjected to Alkali-Silica Reactions," *Construction and Building Materials*, V. 7, No. 2, 1993, pp. 109-115. doi: 10.1016/0950-0618(93)90040-J

8. Schmidt, J. W.; Hansen, S. G.; Barbosa, R. A.; and Henriksen, A., "Novel Shear Capacity Testing of ASR Damaged Full Scale Concrete Bridge," *Engineering Structures*, V. 79, 2014, pp. 365-374. doi: 10.1016/j.engstruct.2014.08.027

9. Barbosa, R. A.; Hansen, S. G.; Hoang, L. C.; and Hansen, K. K., "Residual Shear Strength of a Severely ASR-Damaged Flat Slab Bridge," *Engineering Structures*, V. 161, 2018, pp. 82-95. doi: 10.1016/j.engstruct.2018.01.056

10. Ng, K. E., and Clark, L. A., "Punching Tests on Slabs with Alkali-Silica Reaction," *Structural Engineering*, V. 70, No. 14, 1992, pp. 245-252.

11. Clayton, N.; Currie, R. J.; and Moss, R. M., "The Effects of Alkali-Silica Reaction on the Strength of Prestressed Concrete Beams," *Structural Engineering*, V. 68, No. 16, 1990, pp. 287-292.

12. Ahmed, T.; Burley, E.; and Rigden, S., "The Static and Fatigue Strength of Reinforced Concrete Beams Affected by Alkali-Silica Reaction," *ACI Materials Journal*, V. 95, No. 4, July-Aug. 1998, pp. 356-368.

13. Deschenes, D. J.; Bayrak, O.; and Folliard, K. J., "ASR/DEF – Damaged Bent Caps: Shear Tests and Field Implications," Technical Report for the Texas Department of Transportation, 2009, 271 pp.

14. Habibi, F.; Sheikh, S. A.; Vecchio, F. J.; and Panesar, D., "Effects of Alkali-Silica Reaction on Concrete Squat Shear Walls," *ACI Structural Journal*, V. 115, No. 5, Sept. 2018, pp. 1329-1339. doi: 10.14359/51702238

15. ASTM C1293-09, "Standard Test Method for Determination of Length Change Due to Alkali-Silica Reaction," ASTM International, West Conshohocken, PA, 2009, 7 pp.

16. Rogers, C., and MacDonald, C. A., "The Geology, Properties and Field Performance of Alkali-Aggregate Reactive Spratt, Sudbury and Pittsburg Aggregate Distributed by the Ontario Ministry of Transportation," *14th International Conference on Alkali-Aggregate Reaction*, Austin, TX, 2012, 10 pp.

17. Hooton, R. D.; Rogers, C.; MacDonald, C. A.; and Ramlochan, T., "Twenty-Year Field Evaluation of Alkali-Silica Reaction Mitigation," *ACI Materials Journal*, V. 110, No. 5, Sept.-Oct. 2013, pp. 539-548.

18. Fournier, B.; Rogers, C.; and MacDonald, C. A., "Multilaboratory Study of the Concrete Prism and Accelerated Mortar Bar Expansion Tests with Spratt Aggregate," *14th International Conference on Alkali-Aggregate Reaction*, Austin, TX, 2012, 10 pp.

19. Gautam, B. P.; Panesar, D. K.; Sheikh, S. A.; and Vecchio, F. J., "Effect of Multiaxial Stresses on Alkali-Silica Reaction Damage of Concrete," *ACI Materials Journal*, V. 114, No. 4, July-Aug. 2017, pp. 595-604. doi: 10.14359/51689617

20. Vecchio, F. J., "Shear Rig Design," master's thesis, University of Toronto, Toronto, ON, Canada, 1979, 246 pp.

21. Vecchio, F., and Collins, M., "The Modified Compression Field Theory for Reinforced Concrete Elements Subjected to Shear," *ACI Journal Proceedings*, V. 83, No. 2, Mar.-Apr. 1986, pp. 219-231.

22. Ferche, A. C., "Behaviour and Modelling of ASR-Affected Shear-Critical Reinforced Concrete Structures," PhD dissertation, Department of Civil and Mineral Engineering, University of Toronto, Toronto, ON, Canada, 2020, 392 pp.

23. Mattock, A. H., "Flexural Strength of Prestressed Concrete Sections by Programmable Calculator," *PCI Journal*, V. 24, No. 2, 1964, pp. 13-57.

24. Collins, M. P., and Mitchell, D., *Prestressed Concrete Structures*, Response Publications, Toronto, ON, Canada, 1997, 766 pp.

25. ACI Committee 318, "Building Code Requirements for Structural Concrete (ACI 318-19) and Commentary (ACI 318R-19)," American Concrete Institute, Farmington Hills, MI, 2019, 624 pp.